Macromolecular Chemistry and Physics
www.mcp-journal.de

ABA Type Amphiphiles with Poly(2-benzhydryl-2-oxazine) Moieties: Synthesis, Characterization and Inverse Thermogelation

*Lukas Hahn, Larissa Keßler, Lando Polzin, Lars Fritze, Stefan Forster, Holger Helten, and Robert Luxenhofer**

Thermoresponsive polymers are frequently involved in the development of materials for various applications. Here, polymers containing poly(2-benzhydryl-2-oxazine) (pBhOzi) repeating units are described for the first time. The homopolymer pBhOzi and an ABA type amphiphile comprising two flanking hydrophilic A blocks of poly(2-methyl-2-oxazoline) (pMeOx) and the hydrophobic aromatic pBhOzi central B block (pMeOx-*b*-pBhOzi-*b*-pMeOx) are synthesized and the latter is shown to exhibit inverse thermogelling properties at concentrations of 20 wt.% in water. This behavior stands in contrast to a homologue ABA amphiphile consisting of a central poly(2-benzhydryl-2-oxazoline) block (pMeOx-*b*-pBhOx-*b*-pMeOx). No inverse thermogelling is observed with this polymer even at 25 wt.%. For 25 wt.% pMeOx-*b*-pBhOzi-*b*-pMeOx, a surprisingly high storage modulus of ≈22 kPa and high values for the yield and flow points of 480 Pa and 1.3 kPa are obtained. Exceeding the yield point, pronounced shear thinning is observed. Interestingly, only little difference between self-assemblies of pMeOx-*b*-pBhOzi-*b*-pMeOx and pMeOx-*b*-pBhOx-*b*-pMeOx is observed by dynamic light scattering while transmission electron microscopy images suggest that the micelles of pMeOx-*b*-pBhOzi-*b*-pMeOx interact through their hydrophilic coronas, which is probably decisive for the gel formation. Overall, this study introduces new building blocks for poly(2-oxazoline) and poly(2-oxazine)-based self-assemblies, but additional studies will be needed to unravel the exact mechanism.

1. Introduction

Materials chemistry and design can be used to develop smart materials that react to external stimuli and thus adapt or change their properties. In recent decades, many new materials and polymers have been developed that respond to various stimuli.[1–3] A controlled chemical reaction,[4] modification of polymer properties by changing the temperature,[5] the pH,[6] the absorption of electromagnetic radiation[7] or the action of mechanical,[8] magnetic,[9] or electrical forces[10] have been described in the literature. More specifically, thermoresponsive polymers change their properties by changing temperature beyond critical transition temperature. Turbidity effects, precipitation, and in some cases gelation can be observed. In addition to biomedicine,[11] these properties are also used in separation science,[12] water purification,[13] and optical devices.[14] The thermoresponsive transitions arise from various changes in polymer–polymer and polymer–solvent interactions at different temperatures. A lower critical solution temperature (LCST) system is characterized by a miscible

L. Hahn, L. Keßler, L. Polzin, S. Forster, R. Luxenhofer
Functional Polymer Materials, Chair for Advanced Materials Synthesis, Institute for Functional Materials and Biofabrication, Department of Chemistry and Pharmacy
Julius-Maximilians-University Würzburg
Röntgenring 11, Würzburg 97070, Germany
E-mail: robert.luxenhofer@helsinki.fi

L. Keßler, R. Luxenhofer
Soft Matter Chemistry, Department of Chemistry and Helsinki Institute of Sustainability Science, Faculty of Science
University of Helsinki
P.O. Box 55, Helsinki 00014, Finland

L. Fritze, H. Helten
Institute of Inorganic Chemistry and Institute for Sustainable Chemistry & Catalysis with Boron (ICB)
Julius-Maximilians-University Würzburg
Am Hubland, Würzburg 97074, Germany

The ORCID identification number(s) for the author(s) of this article can be found under https://doi.org/10.1002/macp.202100114

DOI: 10.1002/macp.202100114

polymer-solvent phase and strong polymer–solvent interactions below a certain temperature, which abruptly phase separates above that critical temperature.[15] The opposite is observed in upper critical solution temperature (UCST) systems with relatively weak polymer–solvent interactions, wherein the polymer–polymer interactions exceed polymer–solvent interactions below a critical transition temperature.[15] In aqueous solution, most described systems fall into the LCST category, due to polar moieties in the polymer and hydrogen-bonding capability between polymers and water molecules. In general, non-covalent interactions play a decisive role in the solvation and self-assembly of synthetic and natural polymers. Hydrogen bonding,[16] π–π stacking,[17] dipole–dipole,[18] metal–ligand coordination,[19] or hydrophobic interactions[20] have been established to study and direct the self-assembly of polymers in solution, and to modulate their responsiveness.

Controlled—ideally living—copolymerization is critical to access well-controlled polymer architectures to study defined self-assembly. Living cationic ring-opening polymerization of cyclic imino ethers gives the pseudo-polypeptides of poly(2-oxazoline)s (POx) and poly(2-oxazine)s (POzi), which have seen attention in the past decades as biomaterials in drug delivery and more recently in tissue engineering and biofabrication.[21,22] The LCST type behavior of POx and POzi is well understood.[23–26] The living character of the polymerization allows the synthesis of tailor-made block copolymers with pronounced amphiphilic character leading to self-assembly into spherical[27] or cylindrical micelles[28] and vesicles.[29] Inspired by the family of (thermogelling) Pluronics, Zahoranova et al. synthesized a polymer library of ABA and BAB triblock copolymers based on the hydrophilic poly(2-methyl-2-oxazoline) (pMeOx) (A) and thermoresponsive poly(2-*n*-propyl-2-oxazoline) (p*n*PrOx) (B), but no thermogelation was observed at the investigated temperature range of 10–50 °C.[30] In contrast, the ABA triblock copolymer comprising of poly(2-*iso*-butyl-2-oxazoline) (p*i*BuOx) (B) undergoes reversible sol/gel transition upon heating at 20 wt.%.[31] The hydrogel exhibited a low yield stress in combination with a relatively soft character. Hoogenboom and Monnery described a BAB triblock copolymer bearing p*n*PrOx (B) and hydrophilic poly(2-ethyl-2-oxazoline) blocks (A), which undergoes thermogelation, but only at extremely high degrees of polymerization.[32] In contrast to POx, an additional methylene group in the polymer backbone characterizes the polymer class POzi. The additional CH_2 group modifies the polymers physicochemical properties. In 2017, the first thermogelling POx/POzi-based block copolymer was described using a poly(2-*n*-propyl-2-oxazine) (p*n*PrOzi) block, and cytocompatible and printable physical hydrogels with storage modulus of ≈5 kPa at 20 wt.% polymer concentration were obtained.[33]

For decades, one dominant hydrophobic building block to study self-assembly of amphiphilic POx was poly(2-phenyl-2-oxazoline) (pPheOx).[34,35] More recently, poly(2-benzyl-2-oxazoline) (pBzOx) has been introduced as the hydrophobic block B in ABA triblock copolymers and studied for the solubilization of hydrophobic active pharmaceutical ingredients and natural compounds.[36–38] Since, additional aromatic hydrophobic B blocks have been introduced, specifically poly(2-phenyl-2-oxazine) (pPheOzi) and poly(2-benzyl-2-oxazine) (pBzOzi).[39] The difference between these building blocks is one methylene group in the polymer backbone and/or polymer side chain, allowing to study effects of these small structural changes on its physicochemical properties. Specifically, the rheological properties of aqueous solutions were investigated depending on concentration and temperature. Interestingly, out of the set of four polymers, only pMeOx-*b*-pPheOzi-*b*-pMeOx undergoes reversible inverse thermogelation, that is, it forms a gel upon cooling. This unusual gelation is apparently caused by an order–order transition from spherical- (sol state) to worm-like micelles (gel state), which apparently only occurs for the specific combination of relatively flexible POzi backbone and rigid phenyl sidechain in pPheOzi moieties. Here, we extend the molecular toolkit with respect to aromatic building blocks of POx and POzi by introducing the monomers 2-benzhydryl-2-oxazoline (BhOx) and 2-benzhydryl-2-oxazine (BhOzi), their respective block copolymer amphiphiles, and BhOzi homopolymer. The thermoresponsive properties at different polymer concentrations were analyzed and compared. Interestingly, an inverse thermogelation was once again observed for the POzi-based system while the POx-based polymer did not form a gel.

2. Experimental Section

2.1. Materials and Methods

The substances and reagents in this study were purchased from Sigma-Aldrich (Steinheim, Germany) or TCI-chemicals (Eschborn, Germany) and used without further purification unless otherwise stated. If this was not the case, it will be explicitly mentioned. All substances used for polymerization, specifically methyl trifluoromethylsulfonate (MeOTf) and MeOx were refluxed over CaH_2 for several hours and distilled prior to use. The solvent benzonitrile (PhCN) was dried over phosphorus pentoxide. All dried reagents were stored under dried and inert conditions. The monomers BhOx and BhOzi were recrystallized using methanol followed by co-distillation (three times) with toluene under inert conditions.

2.1.1. Nuclear Magnetic Resonance

Nuclear magnetic resonance (NMR) experiments were performed on a Bruker Fourier 300 (^{1}H: 300.12 MHz) spectrometer at 298 K from Bruker BioSpin (Rheinstetten, Germany) and calibrated using the solvent signals. Multiplicities of signals were depicted as follows: s, singlet; d, doublet; t, triplet; m, multiplet; b, broad.

2.1.2. Gel Permeation Chromatography

Gel permeation chromatography (GPC) was performed on an OMNISEC RESOLVE combined with an OMNISEC REVEAL from Malvern Panalytical using DMF as solvent as described elsewhere.[40] Conventional calibration was performed with poly(methyl methacrylate) (PMMA) standards. The system was kept at 45 °C and a flow rate of 1 mL min^{-1} was used. A precolumn (Dguard), a D2000, and a D3000 column from Malvern were used in series. All samples were filtered through 0.2 µm PTFE filters, Roth (Karlsruhe, Germany).

2.1.3. X-Ray Diffraction

Crystals suitable for single-crystal X-ray diffraction were selected, coated in perfluoropolyether oil, and mounted on MiTeGen sample holders. Diffraction data were collected on Bruker X8 Apex II 4-circle diffractometers with CCD area detectors using Mo-K_α radiation. The crystals were cooled using an Oxford Cryostreams low-temperature device. Data were collected at 100 K. The images were processed and corrected for Lorentz-polarization effects and absorption as implemented in the Bruker software packages. The structures were solved using the intrinsic phasing method (SHELXT)[41] and Fourier expansion technique. All non-hydrogen atoms were refined in anisotropic approximation, with hydrogen atoms "riding" in idealized positions, by full-matrix least squares against F2 of all data, using SHELXL[42] software and the SHELXLE graphical user interface.[43] Other structural information was extracted using OLEX2 software.[44]

2.1.4. Thermogravimetric Analysis

Thermogravimetric analysis (TA) was performed on TG 209 F1 IRIS, NETZSCH (Selb, Germany). The freeze-dried polymer samples (10–15 mg) were placed in aluminum oxide crucibles (NETZSCH Selb, Germany) and heated under synthetic air from 30 to 900 °C with the constant heating rate of 10 K min^{-1}.

2.1.5. Differential Scanning Calorimetry

Differential scanning calorimetry (DSC) was performed on DSC 204 F1 Phoenix equipped with a CC200 F1 Controller (NETZSCH, Selb, Germany). The dynamic scans were recorded using a constant N_2 atmosphere with a heating rate of 10 K min^{-1} (25 – 200 °C) and subsequently cooled to −50 °C (10 K min^{-1}). Two heating and cooling cycles from −50 to 200 °C (10 K min^{-1}) were performed. The samples were placed into aluminum crucibles.

2.1.6. Dynamic Light Scattering

Dynamic light scattering (DLS) experiments were performed using an ALV CGS-3 multi detection goniometry system (Langen, Germany) equipped with a He–Ne laser (632.8 nm) and eight optical avalanche photodiode detectors with an detector angle distance of 16° (correlation time 45 s, 3 runs). Scattering angles between 41° and 147° were measured in four angle sets and a 5° angle interval for each detector (27 angles) at 15, 25, and 40 °C. Prior to each measurement, samples were filtered in dust-free cuvettes using Millex-LG 0.2 µm filters under laminar flow. The polymer concentration was 0.3 g L^{-1} (2 mM aqueous $NaNO_3$ as selective solvent was used). All samples were stored for 24 h at measuring temperature. Additionally, 10 g L^{-1} samples in acetonitrile (unselective solvent) were also investigated at 25 °C and compared. The decay of the electric field-time autocorrelation function (ACF) was fitted using triexponential fit functions (Equation 1) as described previously.[37]

$$g_1(t) = a_1 \cdot e^{\left(-\frac{t}{\tau_1}\right)} + a_2 \cdot e^{\left(-\frac{t}{\tau_2}\right)} a_3 \cdot e^{\left(-\frac{t}{\tau_3}\right)} \quad (1)$$

With the amplitude a_i, decay times $\tau_i = \frac{1}{q^2 \cdot D_i}$, and the absolute value of the scattering vector q. In the case of polydispersity, the Brownian diffusion coefficient D was obtained by extrapolation to zero angle and in the limit of high dilution given by

$$\langle D \rangle_z^{-1} = \frac{\sum_i a_i}{\sum_i a_i \cdot D_i^{-1}} \quad (2)$$

Using the Stokes–Einstein equation, the hydrodynamic radii R_h were obtained

$$R_h = \frac{k_B \cdot T}{6 \cdot \pi \cdot \eta \cdot D} \quad (3)$$

with k_B being the Boltzmann constant, η the viscosity of the solvent, and T the temperature (15, 25, or 40 °C).

Furthermore, the 89° data were fitted using the cumulant method to obtain the polydispersity index (PDI) at different temperatures.

2.1.7. Rolling Ball Viscosity

Rolling ball viscosity experiments were performed on a LOVIS 2000M microviscometer from Anton Paar (Graz, Austria) using a LOVIS 1.8 capillary and a steel ball of 1.5 mm diameter. Prior to the viscosity measurements, the density for every sample was determined at 5 and 40 °C using a DMA 4100 M density meter from Anton Paar (Graz, Austria). A temperature scan from 40 °C → 5 °C and 5 °C → 40 °C of different aqueous sample was performed to establish the temperature-dependent dynamic viscosity.

2.1.8. Rheology

Rheology studies were recorded on an Anton Paar (Ostfildern, Germany) Physica MCR 301 system utilizing a plate–plate geometry (25 mm diameter) equipped with a solvent trap and Peltier element for temperature control. All aqueous samples were measured after complete dissolution in deionized (DI) water at different concentrations at 5 °C. For investigations of viscoelastic behavior, the linear viscoelastic (LVE) region was determined by performing an amplitude sweep (0.01% → 500%) strain deformation using a fixed angular frequency of 10 rad s^{-1}. An oscillatory shear stress sweep (amplitude sweep) can also be used to determine the yield point, yield zone, and flow point. Leaving the LVE region is characterized as yield point. The flow point is defined as $G' = G''$. The region between yield point and flow point is defined as yield zone. A frequency sweep (0.1 rad s^{-1} → 100 rad s^{-1}) was performed at fixed strain deformation of 0.1%. For steady shear experiments, the control shear rate mode was used (0.01 s^{-1} → 100 s^{-1}). The pronounced viscosity η decrease was fitted using the power-law expression (Equation 4).

$$\eta = K \cdot (\dot{\gamma})^{n-1} \quad (4)$$

where K is the consistency index and n the flow index.

2.1.9. Transmission Electron Microscopy

For transmission electron microscopy (TEM) experiments, the polymers were dissolved in DI water to a final concentration of 20 g L^{-1} and stored in the fridge. 400 mesh copper–rhodium grids (maxtaform) with a homemade carbon layer were glow discharged in air for 1.5 min at medium power in a Harrick PDC-002 plasma cleaner. The 20 g L^{-1} sample was diluted (1/125 or 1/625) and 8 µL were incubated on the grids for 1 min before blotting (Whatman filter paper No 50). The grids were washed with water (three times) and with 2% w/v uranyl acetate (three times). A single-tilt room temperature holder in an FEI Tecnai T12 Spirit transmission electron microscope equipped with a LaB_6 emitter at 120 kV was used. Images were recorded with an Eagle CCD camera under low-dose conditions. The micrographs were binned two times resulting in a pixel size of 2.2 Å per pixel at specimen level.

2.2. Synthesis Procedure

2.2.1. Monomer Synthesis

The monomer synthesis of BhOx and BhOzi were carried out as described by Witte and Seeliger[45] with a different workup procedure. For the reaction 1 equiv. of diphenylacetonitrile, 1.2 equiv. of amino-ethanol or amino-propanol and catalytic amounts of zinc acetate dihydrate were added and heated to 130 °C under reflux for several days until the reaction mixture turned brown. Reaction progress was controlled by ^{1}H NMR spectroscopy. After completion, the mixture was dissolved in dichloromethane and washed with H_2O (three times). The organic phase was dried with $MgSO_4$ and concentrated. The raw product was purified via vacuum distillation under argon atmosphere to yield colorless crystals. The resulting compounds BhOx and BhOzi were characterized via ^{1}H, ^{13}C NMR spectroscopy and DSC.

2.2.2. Homopolymer Synthesis

The synthesis was performed as described previously for similar polymers.[50] 1 equiv. of the initiator MeOTf was dissolved in PhCN. The monomer BhOzi (50 equiv.) was added. The reaction mixture was stirred for 2 days at 120 °C. After complete monomer consumption, the reaction mixture was precipitated using ice cold diethyl ether. The dried white powder was analyzed using ^{1}H NMR spectroscopy, GPC, TGA, and DSC.

2.2.3. ABA Type Block Copolymer Synthesis

The synthesis and workup procedures were carried out as described previously for similar polymers.[50] In general, 1 equiv. of the initiator MeOTf was added to a dried and argon flushed flask and dissolved in the respective amount of solvent (PhCN). The first monomer MeOx (35 equiv.) was added to the reaction mixture and heated to 100 °C for ≈2 h. After complete monomer consumption, the mixture was cooled to room temperature and the monomer for the second block BhOx or BhOzi (10 equiv.) was added. The reaction mixture was heated to 120 °C overnight. After complete monomer consumption was confirmed, the third block MeOx (35 equiv.) was added and stirred for 2 h at 100 °C. Termination was carried out by the addition of 3 equiv. of 1-Boc-piperazine (PipBoc) at 50 °C and kept on stirring for 6 h. The solvent was removed at reduced pressure. The raw product was dissolved in DI water. The polymer solution was dialyzed (MWCO 1 kDa, cellulose acetate) against DI water for 3 days. The polymer solution was lyophilized and obtained as a white powder.

3. Results and Discussion

3.1. Monomer Synthesis

The synthesis of the monomers was carried out according to a well-known route established by Witte and Seeliger.[45] The monomer BhOx (Figure S1, Supporting Information) was already synthesized by Culbertson in 2000.[46] It was further converted to a bisoxazoline and then the first ring-opening reactions were carried out. As far as we know, the substance has not yet been used for the cationic ring-opening polymerization. After purification, the monomer was obtained as a colorless crystalline solid with a melting point comparable to the literature (110 °C, lit: 107–109 °C)[46] (Figure S3, Supporting Information). The substance was further analyzed by ^{1}H- and ^{13}C NMR spectroscopy (Figure S2, Supporting Information). In contrast, to the best of our knowledge, the monomer BhOzi (Figure S4, Supporting Information) has not yet been described in the literature.

It is also readily accessible by the Witte and Seeliger method (**Figure 1**A). After purification the structure was verified by ^{1}H- and ^{13}C NMR (Figure 1B and Supporting Information). The additional methylene group (Signal **e** in Figure 1A,B) leads to a significantly higher melting point of 132 °C compared to the 2-oxazoline monomer (Figure 1C). The solid-state structure of BhOzi was determined by single-crystal X-ray diffraction (**Figure 2**). It should be noted that only very recently the first crystal structure of any 2-oxazoline and 2-oxazoline used for cationic ring-opening polymerization was reported. Heck et al. reported this for monomers with pending thiophene groups.[47] The compound crystallizes from a mixture of *n*-hexane and dichloromethane in the monoclinic centrosymmetric space group C 1 2/c 1 (Table S1, Supporting Information). The oxazine ring shows a rotational disorder, with occupancies of 0.609(5) and 0.291(5), which describes a 180° rotation of the ring. No evidence of $\pi-\pi$ stacking was observed in the extended structure, probably due to the star-shaped orientation of the three rings (Figure S5, Supporting Information).

3.2. Polymer Synthesis

A first homopolymer was synthesized using the novel BhOzi monomer by living cationic ring-opening polymerization (**Figure 3**A). ^{1}H NMR analysis after purification verified the polymerization and all relevant peaks could be assigned to the polymer structure Me-poly(2-benzhydryl-2-oxazine)$_{50}$-ω-BocPip (Figure 3B and Figure S6, Supporting Information). An essentially monomodal mass distribution with a minor high molar mass shoulder gave rise to a low dispersity ($Đ = M_w/M_n$: 1.09) (Figure 3C).

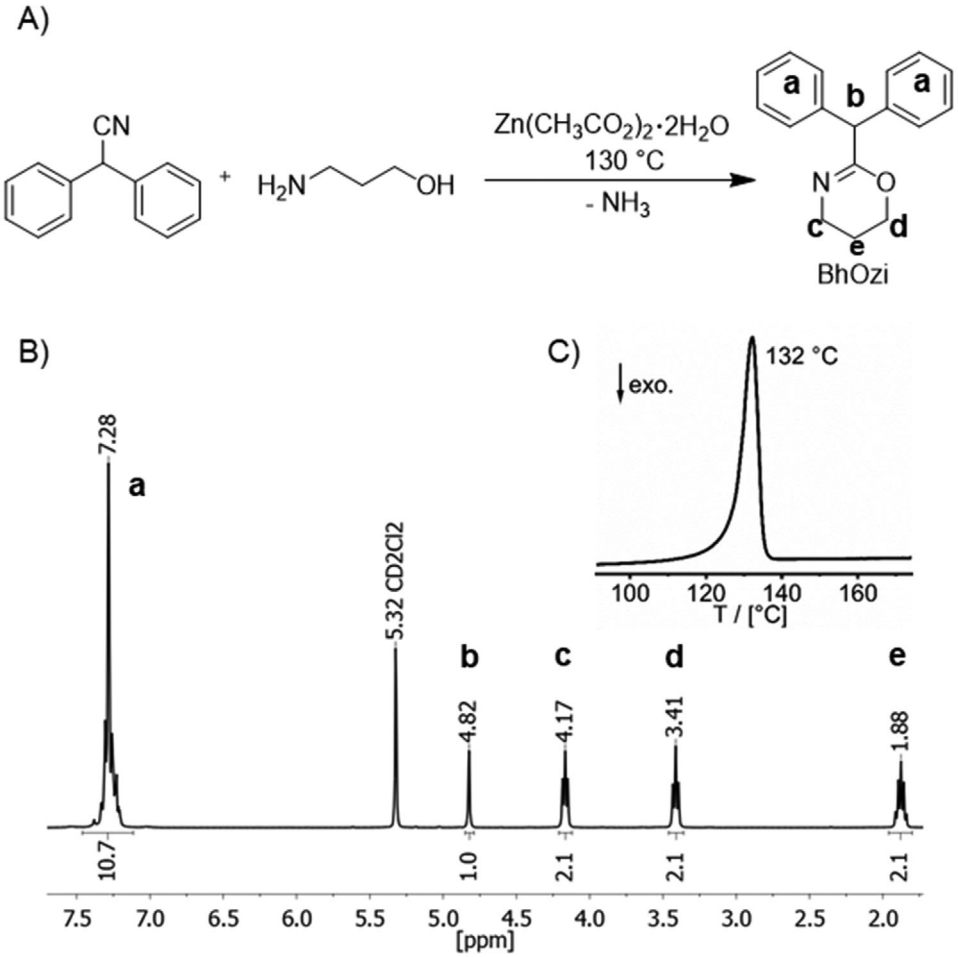

Figure 1. Synthesis of 2-benzhydryl-2-oxazine (BhOzi). A) Synthesis route for BhOzi and B) ^{1}H NMR of BhOzi in CD_2Cl_2 with the assignment of all relevant peaks. C) Differential scanning calorimetry graph shows the melting point of the crystalline solid (m_p: 132 °C).

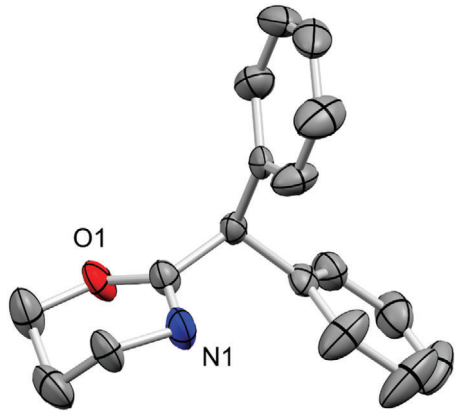

Figure 2. Crystal structure of BhOzi with labeling of heteroatoms. H atoms and disorders are omitted for clarity.

Thermogravimetric analysis showed good thermal stability up to 330 °C, followed by a two-step composition process, which is well known for various POx and POzi (Figure 3D). The polymer appears fully amorphous with a glass transition temperature of 104 °C (Figure 3E). In our ongoing endeavor to understand the structure–property relationship of self-assembly of ABA triblock copolymers for use in drug-delivery systems and hydrogel platforms, we synthesized an ABA type amphiphile with pMeOx A blocks and pBhOzi B blocks (Figure S11, Supporting Information) by using a well-established strategy (**Figure 4**A). ^{1}H NMR analysis confirmed the polymer structure of Me-pMeOx$_{40}$-*b*-pBhOzi$_{14}$-*b*-pMeOx$_{40}$-BocPiP (Figure 4B) and a near monomodal mass distribution with a small but noticeable tailing was obtained from GPC analysis, which may be explained by undesired premature termination of a small fraction of the polymers (Figure 4C). DSC analysis showed one defined T_g of 81.3 °C confirming an amorphous polymer structure without significant micro phase separation of individual polymer blocks. Comparing to previously synthesized similar polymers bearing slightly different aromatic cores similar T_g values were obtained.[37]

3.3. Thermoresponsive Properties in Aqueous Solutions

Surpassing a critical concentration (c_{gel}), self-assembled aggregates can lead to an increase of viscosity and the formation of a

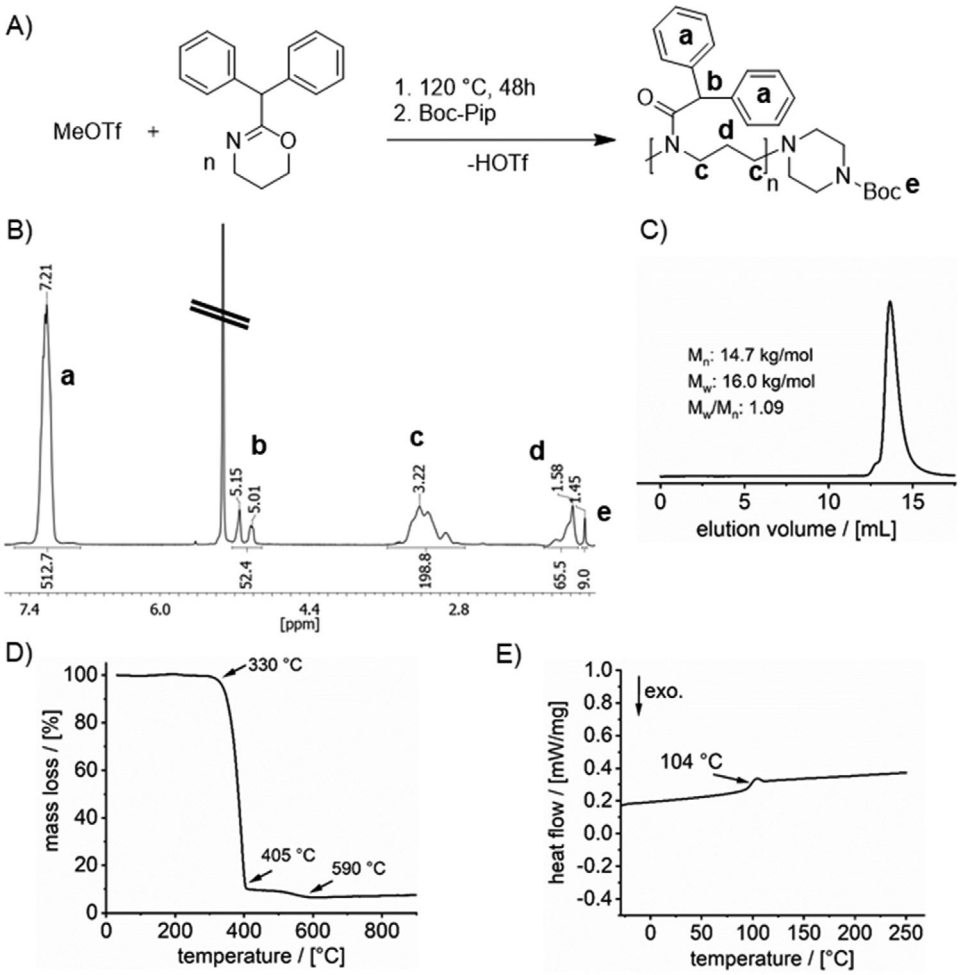

Figure 3. Synthesis of poly(2-benzhydryl-2-oxazine (pBhOzi). A) Schematic illustration of the polymer synthesis. B) ^{1}H NMR of the polymer in CD_2Cl_2 (signal 5.32 ppm) with the assignment of all relevant peaks (the signal at 1.45 ppm was set to 9H (Boc group). C) GPC elugram of the homopolymer pBhOzi in DMF. D) TGA analysis of the purified polymer. E) DSC second heating cycle with the assignment of the glass transition temperature T_g: 104 °C.

physically crosslinked hydrogel. In some cases, the aggregation induced gelation showed pronounced response to temperature leading to a reversible sol/gel transition at the critical temperature (t_{gel}). At 17.5 wt.% and below, an aqueous sample showed unremarkable temperature-viscosity profile. In the investigated temperature range of 5 to 40 °C viscosity values for the free flowing liquid of 120 mPas (5 °C) and 23 mPas (40 °C) are obtained (**Figure 5**). Interestingly, a 20 wt.% sample showed pronounced inverse thermogelation. Starting at 40 °C as a low viscous liquid (49 mPas), a steady increasing viscosity was observed by cooling the sample. Surpassing a critical temperature (≈15 °C for 20 wt.% sample) no viscosity value could be detected. In stable hydrogels, the metal ball, which is used in the measurement, becomes stuck and no values can be obtained. Important to note, the sol/gel transition is fully reversible with only little hysteresis.

Recently, we have observed that such thermogelation can be quite sensitive with respect to the side chain and backbone structure. Accordingly, we prepared a comparable polymer amphiphile bearing pBhOx as the hydrophobic block (Figure S7, Supporting Information) and characterized the polymer by ^{1}H NMR (Figure S8, supporting Information), GPC (Figure S9, Supporting Information), and DSC (Figure S10, Supporting Information) analyses. Interestingly, even at very high polymer concentration of 25 wt.% the pMeOx-*b*-pBhOx-*b*-pMeOx showed no inverse thermogelation (Figure S12, Supporting Information). Presumably, the additional methylene unit increases the flexibility of the hydrophobic core, which affects self-assembly or its dynamics, which in turn might be crucial for inverse thermogelation. As mentioned, similar specificities between POx and POzi based polymers with the same side chains have been observed in previous studies.[39] A similar polymer, pMeOx-*b*-pPheOzi-*b*-pMeOx, showed inverse gelation already at 5 wt.%, but the hydrogel formation is very slow in this case (≈1 h) and due to the formation of worm-like micelles in the cold (below 32 °C). Recently a triblock copolymer comprising the aromatic poly(2-phenethyl-2-oxazoline) as the hydrophobic core (pMeOx-*b*-pPhenEtOx-*b*-pMeOx) was introduced, which forms a physical hydrogel by increased correlation between spherical micelles in the cold.[48] In this case, also 20 wt.% was necessary and the critical temperature was slightly higher at about 23 °C. We suspect that the presently investigated pMeOx-*b*-pBhOzi-*b*-pMeOx might gel due to a similar mechanism.

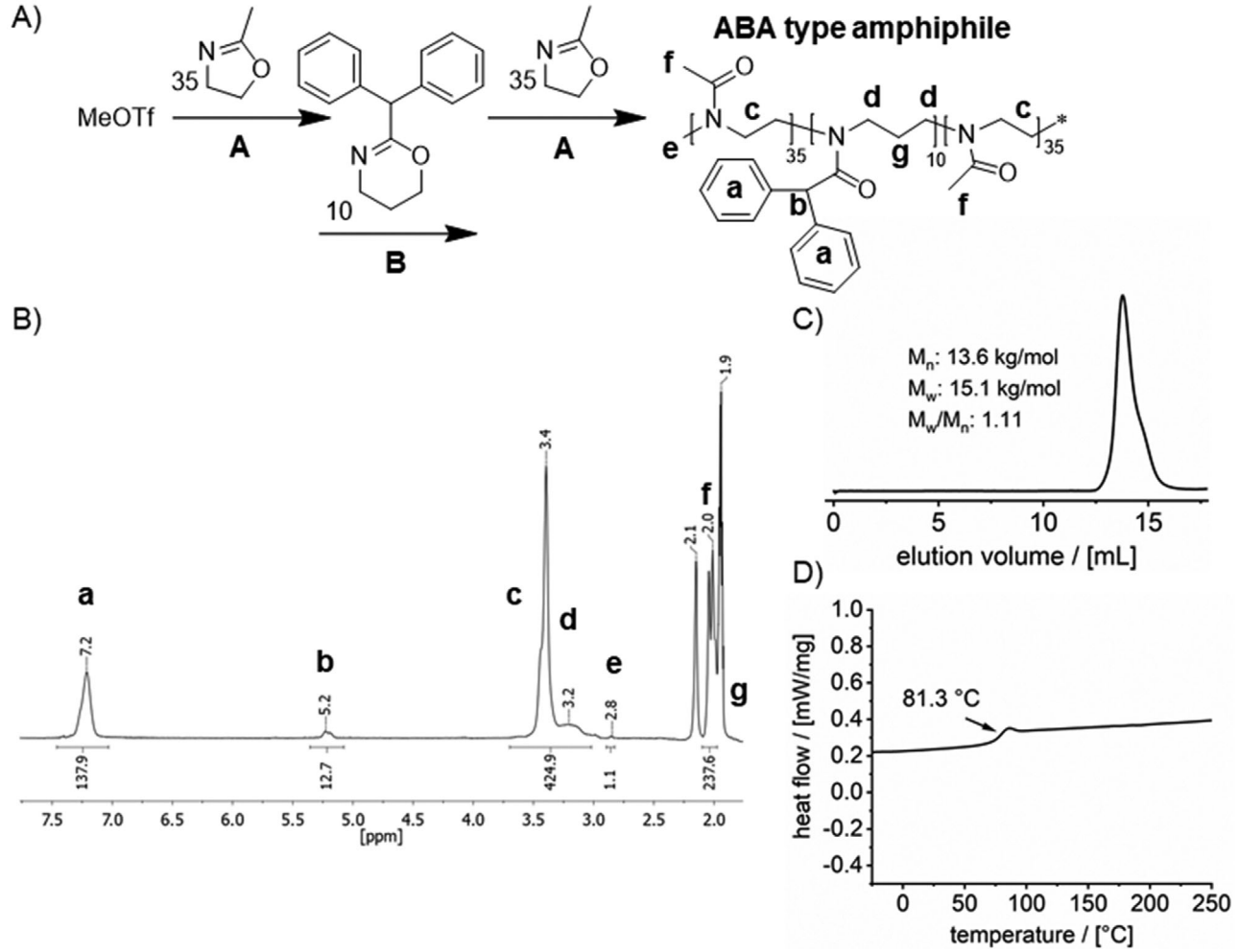

Figure 4. Synthesis of pMeOx-*b*-pBhOzi-*b*-pMeOx amphiphile. A) Scheme of synthesis. B) ^{1}H NMR of the purified amphiphile in CD_3CN (1.94 + 2.2 ppm) with the assignment of all relevant peaks. C) GPC elugram in DMF. D) DSC second heating cycle with the assignment of the glass transition temperature T_g: 81.3 °C.

3.4. Rheological Properties of the Hydrogel

The viscoelasticity of different pMeOx-*b*-pBhOzi-*b*-pMeOx concentrations were analyzed using oscillatory rheology. Frequency sweeps at 5 °C and different polymer concentration were compared (**Figure 6**).

At 15 wt.% no values for a storage modulus could be obtained due to fully viscous character of the sample. Increase in concentration to 17.5 wt.% leads to significantly improved G' and G'' values, as described several times for concentrated solutions, and is in agreement with the obtained viscosity values (120 mPas). The 20 wt.% sample showed pronounced viscoelastic solid-like character. However, the system is still highly dynamic leading to $G' < G''$ at low frequencies. At 25 wt.% in the whole investigated frequency range a stable viscoelastic solid-like character was confirmed with almost constant $G' = 19.4 \pm 0.8$ kPa and a pronounced elasticity expressed by a very low loss factor tan δ of 0.04 ± 0.02. As a note, for a 25 wt.% sample of the polymer pMeOx-*b*-pBhOx-*b*-pMeOx, throughout the investigated frequency range $G'' > G'$ which by definition is a viscoelastic fluid (Figure S13, Supporting Information). Using an amplitude sweep, the LVE range of the hydrogel samples ($G' > G''$) can be determined to assess which deformation/shear stress the system can tolerate (**Figure 7**). The end of the LVE region (G' starts to decrease) is defined as the yield point τ_{yield}, followed by the yield zone, which leads to a liquefaction ($G'' > G'$) of the specimen at the flow point τ_{flow} ($G' = G''$).

Table 1. Summary of important key parameter obtained by oscillatory amplitude sweep for a 20 and 25 wt.% hydrogel sample at 5 °C.

c [wt.%]	G'_{LVE} [kPa]	τ_{yield} [Pa]	τ_{flow} [Pa]
20	9.1 ± 0.1	90	350
25	21.8 ± 0.3	480	1300

Average storage modulus G' in kPa in the linear viscoelastic region, yield point τ_{yield} and flow point τ_{flow} in Pa.

Results of the amplitude sweeps are summarized in **Table 1**. Increase in concentration leads to significantly higher values

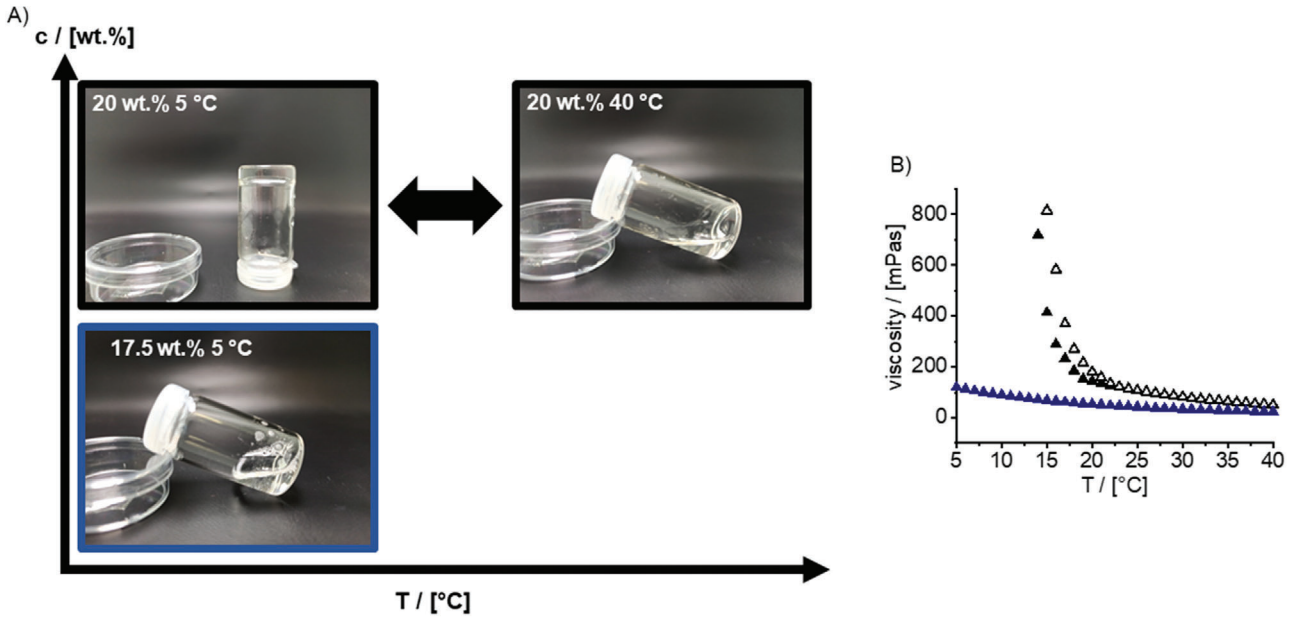

Figure 5. Viscosity of aqueous solutions of pMeOx-*b*-pBhOzi-*b*-pMeOx at 17.5 and 20 wt.%. A) Pictures of the samples at different temperatures (5 and 40 °C). B) Viscosity as a function of temperature investigated using rolling ball viscosity system (filled symbols: cooling, open symbols: heating, blue: 17.5 wt.%, black: 20 wt.%).

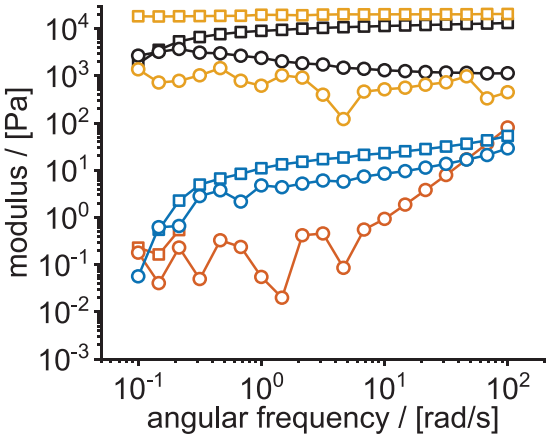

Figure 6. Viscoelasticity of pMeOx-*b*-pBhOzi-*b*-pMeOx aqueous samples at 5 °C and different angular frequencies (squares: storage modulus G', circles: loss modulus G''). Different polymer concentrations (red: 15 wt.%, blue: 17.5 wt.%, black: 20 wt.%, and yellow: 25 wt.%) were tested.

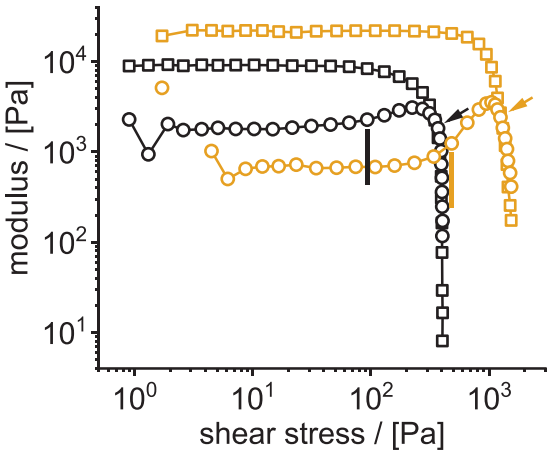

Figure 7. Viscoelasticity of pMeOx-*b*-pBhOzi-*b*-pMeOx aqueous samples (black: 20 wt.% and yellow: 25 wt.%) at 5 °C and different shear stress (squares: storage modulus G', circles: loss modulus G''). The yield point is marked with vertical lines and the flow point with an arrow.

for both parameters. The storage modulus increased more than twice from ≈9 kPa (20 wt.%) to ≈22 kPa. Also, the yield point increased more than fivefold from 90 to 480 Pa.

These values are relatively high in comparison to other POx/POzi-based physical hydrogels at similar concentrations.[31,33,39] Another important rheological parameter is the shear rate-dependent viscosity. The hydrogel exhibited pronounced shear-thinning properties (**Figure 8**). Low shear-thinning indices n, obtained by fitting the values using a power-law expression, characterize the hydrogels as highly shear-thinning materials (n (20 wt.%) = 0.15 ± 0.02, n (25 wt.%) = 0.06 ± 0.001). Increasing the concentration leads to more pronounced shear-thinning properties as evidenced by a decreasing n value. In contrast, the consistency index K increased by increasing concentration (K (20 wt.%) = 201 ± 7, K (25 wt.%) = 1025 ± 4). In general, much higher viscosity values are obtained for the 25 wt.% sample ($\eta_{20\ \mathrm{wt.\%}}$(0.01 1/s) = 9500 Pas, $\eta_{25\ \mathrm{wt.\%}}$ (0.01 1/s) = 81 400 Pas).

3.5. Self-Assembly of ABA Type Amphiphile

Amphiphilic polymers, including POx/POzi-based systems self-assemble into different nanoscale architectures such as spherical

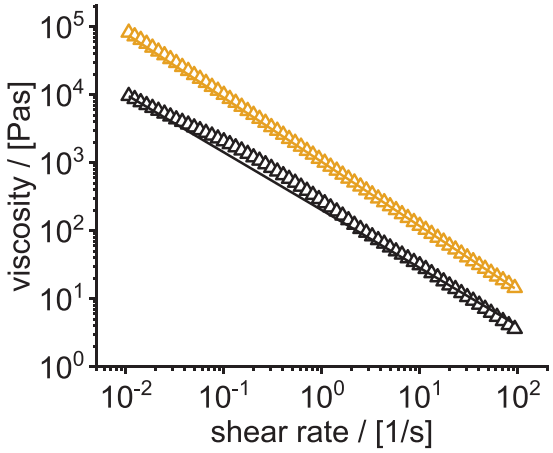

Figure 8. Viscosity as a function of the applied shear rate of pMeOx-*b*-pBhOzi-*b*-pMeOx aqueous samples (black: 20 wt.% and yellow: 25 wt.%) at 5 °C. The shear thinning was fitted using the power-law expression to obtain the flow index *n* and consistency index *K*.

micelles,[28] worm-like micelles[27] or even vesicles.[30,33] Recently, we studied very similar ABA type amphiphiles with various aromatic hydrophobic B blocks.[37,39] At room temperature or above, spherical micelles (8–10 nm) could be detected for all studied systems. Only in one case, for polymers featuring hydrophobic blocks comprising pPheOzi, larger several hundred nanometer sized worm-like aggregates could be detected by DLS experiments and cryogenic TEM at lower temperature. These polymers also showed inverse thermogelation. In addition, a triblock copolymer comprising pPhenEtOx as the hydrophobic block, also showed inverse gelation but did not change the morphology or size of the aggregates upon changes in temperature. However, an enhanced correlation of neighboring micelles was discussed as the driving force for inverse gelation.[48]

To get first insights into the aggregation process of the benzhydryl comprising triblock copolymer that leads to inverse gelation at high concentration, DLS experiments of aqueous solutions of the polymers pMeOx-*b*-pBhOzi-*b*-pMeOx and pMeOx-*b*-pBhOx-*b*-pMeOx were performed (**Table 2**). In the unselective solvent acetonitrile, in which no aggregation is expected, only slightly different hydrodynamic radii for the individual polymer chains were obtained.

The slightly higher value of pMeOx-*b*-pBhOzi-*b*-pMeOx of 2.75 ± 0.02 nm compared to 2.58 ± 0.02 nm of pMeOx-*b*-pBhOx-*b*-pMeOx is consistent with the NMR and GPC results, where slightly higher values for the degree of polymerization and the influence of the additional methylene group in the polymer backbone are also evident. In contrast, in the selective solvent water, the polymers self-assemble into micelles with significant higher hydrodynamic radius. At diluted concentrations needed for DLS and at 25 and 40 °C, the inverse thermogelling polymer pMeOx-*b*-pBhOzi-*b*-pMeOx exhibited micelles with a hydrodynamic radius of 10 nm. Interestingly, the micelles of the polymer pMeOx-*b*-pBhOx-*b*-pMeOx are slightly larger (11.7 and 11.9 nm). At 15 °C, the temperature, at which the gelation at higher concentration actually starts for the polymer pMeOx-*b*-pBhOzi-*b*-pMeOx, the micelle size increased significantly by 2.3 nm. The increase for the non-gelling polymer pMeOx-*b*-pBhOx-*b*-pMeOx was much less

Table 2. Hydrodynamic radii obtained via dynamic light scattering experiments. Measurements were performed on a multi angle device.

Polymer	Acetonitrile [10 g L^{-1}]	aqueous solution [0.3 g L^{-1}]		
	$R_h^{25\,°C}$ [nm] unselective	$R_h^{15\,°C}$ [nm] selective	$R_h^{25\,°C}$ [nm] selective	$R_h^{40\,°C}$ [nm] selective
A-pBhOx-A	2.58* ± 0.02	12.7* ± 0.1 13‡ (0.15)	11.9* ± 0.1 12‡ (0.18)	11.7* ± 0.1 12‡ (0.16)
A-pBhOzi-A	2.75* ± 0.02	12.3* ± 0.2 13‡ (0.26)	10.0* ± 0.1 10‡ (0.11)	10.0* ± 0.1 10‡ (0.09)

The translational diffusion coefficients in dependency of the scattering vector *q* was extrapolated to zero angle (Figure S14, Supporting Information). Using Stokes Equation (3) the hydrodynamic radius was obtained. Error values originate from triexponential fit functions (*) or by cumulant analysis (‡) at 89° which affords the polydispersity index (PDI) given in brackets.

pronounced (0.8 nm). In the whole temperature range, the micelles formed by pMeOx-*b*-pBhOzi-*b*-pMeOx were smaller compared to the pMeOx-*b*-pBhOx-*b*-pMeOx aggregates, respectively.

The described trend can also be observed in the evaluation of the DLS experiments by cumulant method, which gives essentially the same hydrodynamic radii (Table 2). Most interestingly, a significant difference in the development of the dispersity (PDI value) can be observed between the two polymers at different temperatures. In principle, for uniform aggregates in solution the PDI value should approach 0.[49] The gelling polymer A-pBhOzi-A exhibited a relatively high PDI of 0.260 at gelling temperature (15 °C), which decreases rather markedly upon heating to a PDI value of 0.087, indicative of more uniform micelles. The higher value at the gelling temperature could be caused by a minor portion of aggregated micelles due to increased interactions between the micelles or due to an extended correlation of the micelles, ultimately causing the system to gel at higher concentration. Important to note, this temperature-dependent change in PDI values was not observed with the non-gelling polymer. In this case, a very similar PDI in the range of 0.15–0.17 is observed at all temperatures.

The DLS study was performed in non-gelling concentration and therefore does not allow a simple correlation to the situation at higher concentrations. Nevertheless, it is a first indication of the different aggregation of the two amphiphiles. In addition, negative stain TEM images were obtained from a 20 g L^{-1} aqueous solution stored at 5 °C.

The non-gelling polymer pMeOx-*b*-pBhOx-*b*-pMeOx clearly self-assembles into rather uniform spherical micelles (**Figure 9**A,B) similar to previously described non-gelling POx-based polymers with an aromatic hydrophobic block[37] and thermogelling polymer described very recently.[48] Interestingly, even though the self-assemblies formed in the case of the gel-forming polymer pMeOx-*b*-pBhOzi-*b*-pMeOx are also rather uniform and spherical, the overall impression suggests a strongly deviating aggregation behavior (Figure 9C). First, the contrast from the staining reagent is different, which suggests different accessability of the contrast agent and may be attributed to a higher flexibility of the oxazine backbone in the hydrophobic block compared to the non-gelling oxazoline-based polymer. More importantly, however, the TEM images suggest a strong interaction

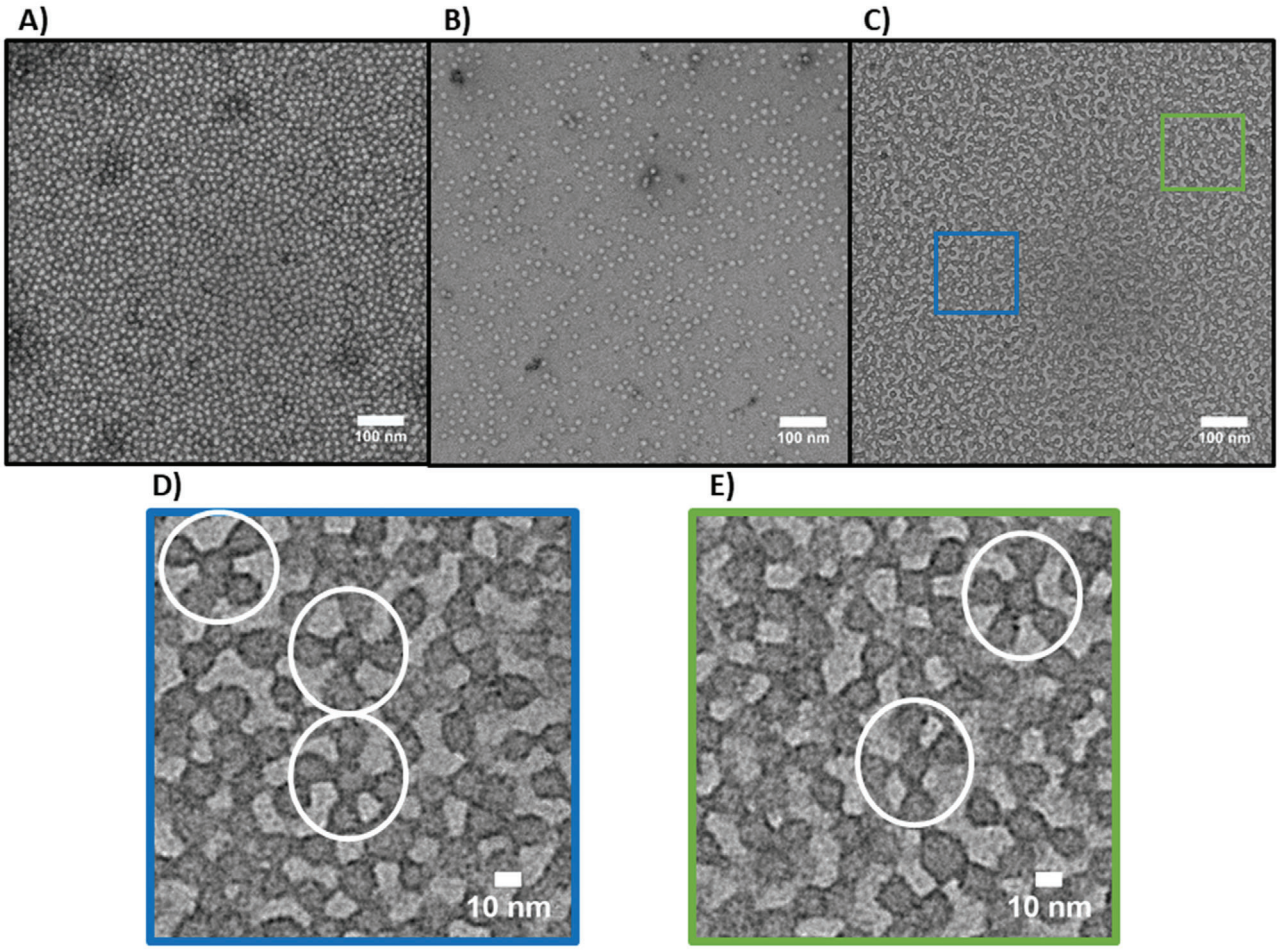

Figure 9. TEM images of pMeOx-*b*-pBhOx-*b*-pMeOx (A, B) and pMeOx-*b*-pBhOzi-*b*-pMeOx (C–E). As staining reagent uranyl acetate was used. A) Image of highly concentrated and B) a more diluted aqueous solution of A-pBhOx-A suggests uniform and non-interacting spherical micelles. C) In contrast, the micrograph of A-pBhOzi-A strongly suggests interacting aggregates of spherical micelles and clustering as highlighted in D and E. D,E) Zoomed view of clustering aggregates. Highlighted in white circles are interesting geometric features which appear common in the image.

tendency among the individual micelles, mediated via the hydrophilic corona, which seems to form sticky patches between the micelles (Figure 9D,E white circles). As a result, a superstructure of self-assemblies is formed, which is likely the underlying reason for the gel formation at high concentration and low temperatures. Interestingly, similar arrangements were not observed in otherwise very similar inverse-gelling POx/POzi platforms,[37,48] which suggest that these structures might be specific for this particular combination of hydrophilic and hydrophobic blocks.

4. Conclusion

Herein we demonstrated the novel aromatic monomers BhOx and BhOzi and their application in a cationic ring-opening polymerization. ABA type amphiphiles with the aromatic hydrophobic central block of pBhOx and pBhOzi are synthesized and compared. Surprisingly, the polymer pMeOx-*b*-pBhOzi-*b*-pMeOx undergoes rapid inverse thermogelation above 20 wt.% while its homologue pMeOx-*b*-pBhOx-*b*-pMeOx does not. The rheological properties of the hydrogel, such as pronounced viscoelastic solid appearance and shear thinning, are confirmed. Minor differences in aggregation for the two amphiphiles were observed by light scattering experiments, of particular interest is the temperature-dependent dispersity observed for pMeOx-*b*-pBhOzi-*b*-pMeOx, which is not observed for pMeOx-*b*-pBhOx-*b*-pMeOx. Interestingly, the gel-forming polymer pMeOx-*b*-pBhOzi-*b*-pMeOx showed unique fusion and ordering of micelles in TEM experiments in comparison to the non-gelling polymer pMeOx-*b*-pBhOx-*b*-pMeOx, in which the micelles are also uniform and spherical, but do not seem to interact. The controlled synthesis, reversible and rapid inverse gelation together with the distinct rheological properties open up a range of applications for this novel hydrogel and extends the toolkit for the recently discovered platform of POx- and POzi-based thermogelling polymers. The gel properties, namely the fast sol/gel transition and shear thinning, are promising for use as sacrificial material in biofabrication, especially in bioprinting, or the storage of biologically sensitive materials such as unstable proteins.

Supporting Information

Supporting Information is available from the Wiley Online Library or from the author.

Acknowledgements

The authors would like to gratefully acknowledge support by the Deutsche Forschungsgemeinschaft (DFG, German Research Foundation)—project number 326998133—TRR 225 (subproject A03) and project number 398461692, awarded to R.L.). H.H. thanks the DFG for support through the Heisenberg Programme (HE 6171/7-1, 401738081). The authors are very grateful for the HDRC-Software version 6.3.1 provided by O. Nirschl and K. Fischer, Physical Chemistry of Polymers at the Johannes Gutenberg University Mainz led by Dr. Sebastian Seiffert (formerly Dr. Manfred Schmidt) for DLS data analysis. Light scattering experiments were possible through support of the Deutsche Forschungsgemeinschaft (INST 93/774-1 FUGG). The authors gratefully acknowledge access to electron microscopy facilities provided by Prof. Bettina Böttcher at the Rudolf Virchow Center, Julius-Maximilians-University Würzburg. In addition, the authors would like to thank Maxim Melnikov, Dario Polzin, and Christian May for technical support and Ilona Paulus for GPC support.

Open access funding enabled and organized by Projekt DEAL.

Conflict of Interest

The authors declare no conflict of interest.

Data Availability Statement

The data that support the findings of this study are openly available in ChemRxiv at https://doi.org/10.26434/chemrxiv.14322194.

Keywords

inverse thermogels, physical hydrogels, poly(2-oxazine), poly(2-oxazoline), self-assembly

Received: March 31, 2021
Revised: June 23, 2021
Published online: August 2, 2021

[1] L. Hu, Y. Wan, Q. Zhang, M. J. Serpe, *Adv. Funct. Mater.* **2020**, *30*, 1903471.
[2] M. A. C. Stuart, W. T. S. Huck, J. Genzer, M. Müller, C. Ober, M. Stamm, G. B. Sukhorukov, I. Szleifer, V. V. Tsukruk, M. Urban, F. Winnik, S. Zauscher, I. Luzinov, S. Minko, *Nat. Mater.* **2010**, *9*, 101.
[3] Z. Shen, F. Chen, X. Zhu, K.-T. Yong, G. Gu, *J. Mater. Chem. B* **2020**, *8*, 8972.
[4] K. T. Kim, J. J. L. M. Cornelissen, R. J. M. Nolte, J. C. M. V. Hest, *J. Am. Chem. Soc.* **2009**, *131*, 13908.
[5] A. P. Constantinou, B. Zhan, T. K. Georgiou, *Macromolecules* **2021**, *54*, 1943.
[6] F. Ofridam, M. Tarhini, N. Lebaz, É. Gagnière, D. Mangin, A. Elaissari, *Polym. Adv. Technol.* **2021**, *32*, 1455.
[7] J. Hrbac, V. Pavelka, J. Crassous, J. Zadny, L. Fekete, J. Pokorny, P. Vanysek, J. Storch, J. Vacek, *Electrochem. Commun.* **2020**, *113*, 106689.
[8] K.-P. Wang, Y.-P. Deng, T. Wang, Q.-D. Wang, C.-G. Qian, X.-Y. Zhang, *Polymer* **2020**, *210*, 123017.
[9] H. Meng, J. Wan, J. Jing, D. Sun, B. Jiang, F. Liang, Z. Yang, *Chin. Chem. Lett.* **2020**, *31*, 253.
[10] C. Rullyani, M. Singh, S.-H. Li, C.-F. Sung, H.-C. Lin, C.-W. Chu, *Org. Electron.* **2020**, *85*, 105818.
[11] F. Doberenz, K. Zeng, C. Willems, K. Zhang, T. Groth, *J. Mater. Chem. B* **2020**, *8*, 607.
[12] A. Kikuchi, T. Okano, *Prog. Polym. Sci.* **2002**, *27*, 1165.
[13] T. Saitoh, K. Asano, M. Hiraide, *J. Hazard. Mater.* **2011**, *185*, 1369.
[14] J. Zhang, G. Pu, M. R. Dubay, Y. Zhao, S. J. Severtson, *J. Mater. Chem. C* **2013**, *1*, 1080.
[15] E. Gruber, in *Polymerchemie: Eine Einführung in die Chemie und Physikalische Chemie der Makromoleküle* (Ed: E. Gruber), Steinkopff, Heidelberg **1980**, p. 70.
[16] X. Hu, M. Vatankhah-Varnoosfaderani, J. Zhou, Q. Li, S. S. Sheiko, *Adv. Mater.* **2015**, *27*, 6899.
[17] A. M. Smith, R. J. Williams, C. Tang, P. Coppo, R. F. Collins, M. L. Turner, A. Saiani, R. V. Ulijn, *Adv. Mater.* **2008**, *20*, 37.
[18] T. Bai, P. Zhang, Y. Han, Y. Liu, W. Liu, X. Zhao, W. Lu, *Soft Matter* **2011**, *7*, 2825.
[19] M. Ahmadi, S. Seiffert, *Soft Matter* **2020**, *16*, 2332.
[20] E. Su, O. Okay, *Eur. Polym. J.* **2017**, *88*, 191.
[21] T. Lorson, M. M. Lübtow, E. Wegener, M. S. Haider, S. Borova, D. Nahm, R. Jordan, M. Sokolski-Papkov, A. V. Kabanov, R. Luxenhofer, *Biomaterials* **2018**, *178*, 204.
[22] A. Zahoranová, R. Luxenhofer, *Adv. Healthcare Mater.* **2021**, *10*, 2001382.
[23] R. Hoogenboom, H. M. L. Thijs, M. J. H. C. Jochems, B. M. Van Lankvelt, M. W. M. Fijten, U. S. Schubert, *Chem. Commun.* **2008**, https://doi.org/10.1039/B813140F.
[24] M. M. Bloksma, R. M. Paulus, H. P. C. Van Kuringen, F. Van Der Woerdt, H. M. L. Lambermont-Thijs, U. S. Schubert, R. Hoogenboom, *Macromol. Rapid Commun.* **2012**, *33*, 92.
[25] S. Huber, R. Jordan, *Colloid Polym. Sci.* **2008**, *286*, 395.
[26] J.-S. Park, K. Kataoka, *Macromolecules* **2007**, *40*, 3599.
[27] A. Schulz, S. Jaksch, R. Schubel, E. Wegener, Z. Di, Y. Han, A. Meister, J. Kressler, A. V. Kabanov, R. Luxenhofer, C. M. Papadakis, R. Jordan, *ACS Nano* **2014**, *8*, 2686.
[28] S. Jaksch, A. Schulz, Z. Di, R. Luxenhofer, R. Jordan, C. M. Papadakis, *Macromol. Chem. Phys.* **2016**, *217*, 1448.
[29] D. Daubian, J. Gaitzsch, W. Meier, *Polym. Chem.* **2020**, *11*, 1237.
[30] A. Zahoranová, M. Mrlík, K. Tomanová, J. Kronek, R. Luxenhofer, *Macromol. Chem. Phys.* **2017**, *218*, 1700031.
[31] M. M. Lübtow, M. Mrlik, L. Hahn, A. Altmann, M. Beudert, T. Lühmann, R. Luxenhofer, *J. Funct. Biomater.* **2019**, *10*, 36.
[32] B. D. Monnery, R. Hoogenboom, *Polym. Chem.* **2019**, *10*, 3480.
[33] T. Lorson, S. Jaksch, M. M. Lübtow, T. Jüngst, J. Groll, T. Lühmann, R. Luxenhofer, *Biomacromolecules* **2017**, *18*, 2161.
[34] B. Trzebicka, N. Koseva, V. Mitova, A. Dworak, *Polymer* **2010**, *51*, 2486.
[35] Y. Milonaki, E. Kaditi, S. Pispas, C. Demetzos, *J. Polym. Sci., Part A: Polym. Chem.* **2012**, *50*, 1226.
[36] Y. Seo, A. Schulz, Y. Han, Z. He, H. Bludau, X. Wan, J. Tong, T. K. Bronich, M. Sokolsky, R. Luxenhofer, R. Jordan, A. V. Kabanov, *Polym. Adv. Technol.* **2015**, *26*, 837.
[37] L. Hahn, M. M. Lübtow, T. Lorson, F. Schmitt, A. Appelt-Menzel, R. Schobert, R. Luxenhofer, *Biomacromolecules* **2018**, *19*, 3119.
[38] M. R. Landry, A. N. Duross, M. J. Neufeld, L. Hahn, G. Sahay, R. Luxenhofer, C. Sun, *Materials Today Bio.* **2020**, *8*, 100082.
[39] L. Hahn, M. Maier, P. Stahlhut, M. Beudert, V. Flegler, S. Forster, A. Altmann, F. Töppke, K. Fischer, S. Seiffert, B. Böttcher, T. Lühmann, R. Luxenhofer, *ACS Appl. Mater. Interfaces* **2020**, *12*, 12445.
[40] J. Blöhbaum, I. Paulus, A.-C. Pöppler, J. Tessmar, J. Groll, *J. Mater. Chem. B* **2019**, *7*, 1782.
[41] G. Sheldrick, *Acta Crystallogr. C* **2015**, *71*, 3.
[42] G. Sheldrick, *Acta Crystallogr. A* **2008**, *64*, 112.

[43] C. B. Hübschle, G. M. Sheldrick, B. Dittrich, *J. Appl. Crystallogr.* **2011**, *44*, 1281.
[44] O. V. Dolomanov, L. J. Bourhis, R. J. Gildea, J. A. K. Howard, H. Puschmann, *J. Appl. Crystallogr.* **2009**, *42*, 339.
[45] H. Witte, W. Seeliger, *Angew. Chem., Int. Ed. Eng.* **1972**, *11*, 287.
[46] B. M. Culbertson, Y. Tong, S. R. Schricker, *Polym. Adv. Technol.* **2000**, *11*, 9.
[47] J. G. Heck, J. Löblein, J. Kade, P. Dalton, R. Luxenhofer, R. Green, *Melt Electrospin Writing (MEW) of Novel Conductive Polymer Composites for Electroactive Fibers* [E-Poster, WBC2020-3735], **2020**. **WBC 2020, Virtual Conference**: p. https://virtual.wbc2020.org/page/e-posters
[48] L. Hahn, E. Karakaya, T. Zorn, B. Sochor, M. Maier, P. Stahlhut, S. Forster, K. Fischer, S. Seiffert, A.-C. Pöppler, R. Detsch, R. Luxenhofer, *Biomacromolecules* **2021**, *22*, 3017.
[49] D. E. Koppel, *J. Chem. Phys.* **1972**, *57*, 4814.
[50] M. M. Lübtow, L. Keßler, A. Appelt-Menzel, T. Lorson, N. Gangloff, M. Kirsch, S. Dahms, R. Luxenhofer, *Macromol. Bioscience* **2018**, *18*, 1800155.

